batteries

Article

Fractional-Order Sliding-Mode Observers for the Estimation of State-of-Charge and State-of-Health of Lithium Batteries

Minghao Zhou [1], Kemeng Wei [1], Xiaogang Wu [1], Ling Weng [2,*], Hongyu Su [1], Dong Wang [1], Yuanke Zhang [1] and Jialin Li [1]

[1] School of Electrical and Electronic Engineering, Harbin University of Science and Technology, Harbin 150080, China; zhouminghao@hrbust.edu.cn (M.Z.)
[2] School of Materials Science and Chemical Engineering, Harbin University of Science and Technology, Harbin 150080, China
* Correspondence: l.weng@hrbust.edu.cn; Tel.: +86-139-0361-7062

Abstract: Lithium batteries are widely used in power storage and new energy vehicles due to their high energy density and long cycle life. The accurate and real-time estimation for the state-of-charge (SoC) and the state-of-health (SoH) of lithium batteries is of great significance to improve battery life, reliability, and utilization efficiency. In this paper, three cascaded fractional-order sliding-mode observers (FOSMOs) are designed for the estimation of SoC by observing the terminal voltage, the polarization voltage, and the open-circuit voltage of a lithium cell, respectively. Furthermore, to calculate the value of the SoH, two FOSMOs are developed to estimate the capacity and internal resistance of the lithium cell. The control signals of the observers are continuous by utilizing fractional-order sliding manifolds without low-pass filters. Compared with the existing sliding-mode observers for SoC and SoH, weaker chattering, faster response, and higher estimation accuracy are obtained in the proposed method. Finally, the experiment tests demonstrate the validity and feasibility of the proposed observer design method.

Keywords: sliding-mode observer (SMO); state-of-charge (SoC); state-of-health (SoH); lithium battery

Citation: Zhou, M.; Wei, K.; Wu, X.; Weng, L.; Su, H.; Wang, D.; Zhang, Y.; Li, J. Fractional-Order Sliding-Mode Observers for the Estimation of State-of-Charge and State-of-Health of Lithium Batteries. *Batteries* **2023**, *9*, 213. https://doi.org/10.3390/batteries9040213

Academic Editor: Matthieu Dubarry

Received: 8 January 2023
Revised: 25 March 2023
Accepted: 29 March 2023
Published: 1 April 2023

1. Introduction

With the depletion of global energy, new energy vehicles are gradually replacing fuel vehicles. Batteries, represented by lithium batteries, are the core components of new-energy vehicles. The real-time estimation for SoC and SoH is vital and indispensable for the safety, reliability, and efficiency of lithium batteries [1,2]. The model of the battery is the mathematical expression of its characteristics, and accurate battery models can not only reflect the relationship between battery characteristics and influencing factors, but also provide an important basis for accurate state estimation. The mathematical models of lithium batteries are generally divided into two types: the electrochemical model [3] and the equivalent circuit model (ECM) [4]. Electrochemical models take into account the impact of the distributed behaviors inside the cells, including the potentials in the electrolyte and the concentration of Li-ions [5]. The equivalent circuit model has been widely used in the modeling and state estimation of various power lithium batteries because of its simple structure, easy integration, easy real-time calculation, and low complexity. In recent years, scholars proposed a variety of equivalent circuit models such as the Rint model, Thevenin model, Partnership for a New Generation of Vehicles (PNGV) model, and Dual Polarization (DP) model. The Thevenin model, also called the RC equivalent circuit model, which consists of an internal resistance and some resistance-capacitance loops, can simulate the static and dynamic performance precisely. However, because of their stochastic internal parameter variations, the uncertainties existing in the lithium batteries would be hard to estimate and compensate practically [6,7]. The main estimation methods for lithium batteries based on ECMs include the impedance measurement method [8], machine learning

algorithm [9], extended Kalman filter (EKF) algorithm [10], and sliding-mode observer-based method [11].

The impedance measurement method can obtain the functional relationship between the SoC and the lithium battery model by stimulating the currents with different frequencies [12]. However, the functional relationship cannot be obtained accurately because the internal resistance of the battery is affected by its temperature and SoH [13], and the measurement can only be carried out when the batteries are off-line [14]. The machine learning algorithm regards the lithium batteries as a black box and performs tests and training only by using a large amount of experimental data, regardless of the battery's internal relations [15]. In [16], the machine learning algorithm is used to estimate the SoC of Li-ion batteries, which achieves high accuracy and fast estimation. However, the process of estimation is extremely reliant on the training number and the count of neurons in the hidden layer. The extended Kalman filter [17] uses the estimation state values of the present moment and the previous moment to observe the currents, while EKF needs precise modeling and other factors such as aging and environmental changes.

Generally, the aforementioned estimation methods of SoC and SoH depend on accurate modeling, however the existing ECMs have their own limitations [18]. The sliding-mode observer (SMO) is insensitive to the internal parameter variations and robust to external disturbances, so it is suitable for the state observation of nonlinear and time-varying systems [19]. In [20], a multi-time scale dual-SMO is designed to estimate the SoC and SoH of lithium batteries simultaneously. Based on Thevenin model, [21] designed a dual sliding-mode observer to observe the SOC and SoH of the battery, but it is difficult to obtain the equivalent control signal by relying on the filter with complex structure. In [22], the estimation of the SoC and SoH state is carried out by comparing the extended Kalman filter with Particle Filtering. It is found that Particle Filtering has higher estimation accuracy. However, it also has high dependence on the model and poor robustness. In [23], the variable parameters discrete sliding-mode observer is proposed in the time-varying circumstance to estimate the SoC of a lithium battery. However, the low availability of data and the phase lag of the low-pass filter (LPF) make the existing SMO have limitations in the practical application. In [24], Alexander used the least square method to estimate the model parameters in the electrochemical model of lithium batteries, considering the aging of lithium batteries. Ref. [25] proposed a sliding-mode observer based on an AEM model to estimate the SoH of a battery, but its control signal is discontinuous, which is not conducive to practical application.

For accurate and real-time estimation, the fractional-order sliding-mode observers are proposed for the SoC and SoH using the RC equivalent circuit model, which not only avoids the phase lag caused by LPF, but also smooths the observation signals by fractional order integrator. Furthermore, the observers are designed in the cascade type for the high accuracy of the global estimation. The contributions of the paper can be summarized as follows:

(1) The accuracy of estimation for SoC and SoH is enhanced without utilizing the LPF. Owing to the fractional-order sliding manifolds, the control signals of the observers are smoothed by the $\alpha + 1$ order integrator, which can be directly used to estimate SoC and SoH.
(2) The accuracy of the data is improved. The proposed FOSMOs adopt the data of measured voltage and current to estimate the significant data, which will be used in the next development of FOSMOs.

This paper is organized as follows: Section 2 introduces the RC equivalent circuit model of lithium batteries. In Section 3, three FOSMOs are designed in the estimation process of SoC. In Section 4, two novel observers are presented in the process of estimation of SoH. Section 5 gives the experimental results. Finally, conclusions are shown in Section 6.

2. Preliminary

2.1. The Mathematical Model of the Battery

The establishment of a high precision mathematical model is the basis of SoC and SoH estimation of lithium batteries. The lithium battery is a typical nonlinear system. The mathematical model of lithium batteries mainly includes the electrochemical model and ECM [26]. The ECM has a simpler structure and lower computational complexity than the electrochemical model [27]. Therefore, the RC equivalent circuit model is widely used in the observation and control of lithium batteries. The RC equivalent circuit model presents different modes according to the SoC, the current, and temperature, and it can simulate the static and dynamic performance of the lithium batteries properly [28]. The RC equivalent circuit model of lithium batteries is shown in Figure 1.

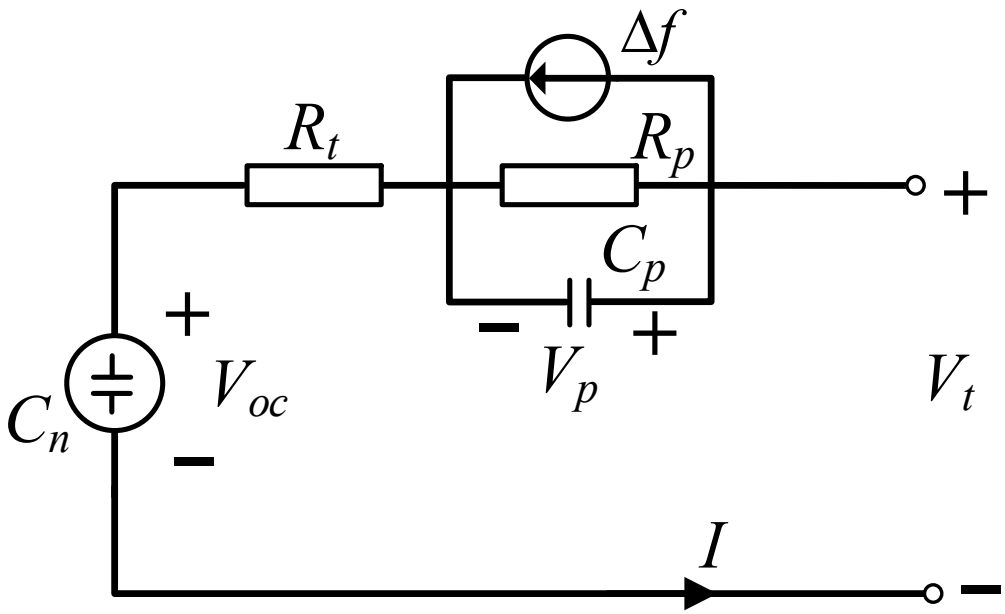

Figure 1. RC equivalent circuit model of the lithium battery.

In Figure 1, the controlled voltage source V_{oc} (Z) is used to describe the open-circuit voltage of the lithium battery. The V_{oc} (Z) and SoC of the battery meet a certain function relationship, and the V_{oc} is affected by the ambient temperature. Z stands for SoC [29]. The internal resistance of the battery is generally uncertain, which contains ohmic resistance R_t and polarization resistance R_p. C_p is the polarization capacitance. The polarization voltage V_p is used to describe the polarization effect of the lithium battery in the charge and discharge processes. The three polarization parameters are jointly affected by the charge and discharge currents, SoC, and ambient temperature. V_t is the terminal output voltage, and Δf represents the uncertainties. The dynamics of the SoC can be expressed as:

$$\dot{Z} = \dot{f}_{voc}^{-1}(V_{oc}) = \frac{I}{C_n} \tag{1}$$

where C_n is the rated capacity. The SoC and the V_{oc} satisfy the following:

$$\dot{V}_{oc} = \dot{f}_{voc}(Z) = \kappa \dot{Z} \tag{2}$$

where the variable κ, the slope at point Z, can be obtained from:

$$\kappa = \frac{\dot{V}_{oc}}{\dot{Z}} = \frac{df_{voc}(Z)}{dZ} \tag{3}$$

where the nonlinear function $f_{voc}(Z)$ is the mapping of V_{oc} versus Z.

The mathematical relationship of V_t, V_{oc}, and V_p in Figure 1 is expressed as:

$$\dot{V}_t = -a_1 V_t + a_1 V_{oc}(Z) + R_t \dot{I} + b_1 I \tag{4}$$

$$\dot{V}_{oc} = \kappa a_2 V_t - \kappa a_2 V_{oc} - \kappa a_2 V_p \tag{5}$$

$$\dot{V}_p = -a_1 V_p + b_2 I + \Delta f \tag{6}$$

where $a_1 = \frac{1}{R_p C_P}$, $a_2 = \frac{1}{R_t C_n}$, $b_1 = \frac{1}{C_n} + \frac{1}{C_P} + \frac{R_t}{R_p C_P}$, $b_2 = \frac{1}{C_P}$. The disturbance Δf is unknown, which is Lipschitz and bounded, then:

$$|\Delta f| \le F_{f1}, \ \left| D^{\alpha+1} \Delta f \right| \le F_{f2} \tag{7}$$

where F_{f1} and F_{f2} are known positive constants. The fractional-order derivate of the estimation error of the open-circuit voltage and the estimation error of the polarization voltage are assumed to be bounded as:

$$\left| D^{\alpha+1} \left(V_{oc} - \hat{V}_{oc} \right) \right| \le F_{oc}, \ \left| D^{\alpha+1} \left(V_p - \hat{V}_p \right) \right| \le F_p \tag{8}$$

where $F_{oc} > 0$ and $F_p > 0$ are certain constants, and $\hat{V}_{oc}$ and $\hat{V}_p$ are the estimations of V_{oc} and V_p.

2.2. High Order Sliding-Mode Observer

The high order sliding-mode control (HOSMC) proposed by Levant in 1996 can eliminate chattering and improve the control accuracy effectively [30]. As a special type of the HOSMC, the super twisting algorithm (STA) can realize convergency of the system state to the ideal sliding manifold $s = \dot{s} = 0$ in finite time, but the rate of the convergence is restricted if the initial state is far away from the equilibrium point [31].

Consider a first-order system as follows:

$$\dot{x} = f(x) + u + d \tag{9}$$

where x is the state variable, $f(x)$ a known function, u the control input of the system, and d the disturbance. Then, a high order sliding-mode observer (HOSMO) [32] can be designed as:

$$\dot{\hat{x}} = f(\hat{x}) + u + v \tag{10}$$

where $\hat{x}$ is the observed value of x, v the observer control signal, and the estimating error is defined as $e = x - \hat{x}$. Then, we can obtain the follow form:

$$\dot{e} = [f(x) - f(\hat{x})] + d - v \tag{11}$$

The finite time convergence of the system is guaranteed if the observer control law is designed as follows:

$$v = -k_1 |e|^{1/2} \mathrm{sgn}(e) - k_2 \int_0^t \mathrm{sgn}(e) dt \tag{12}$$

The system state could converge to the equilibrium point in finite time and the sliding manifold could achieve $s = \dot{s} = 0$.

The lemmas are given below to prove the theorems presented in Sections 3 and 4. To prove the stability of the fractional differential systems, Lemma 1 is given as the theoretical basis to design the fractional-order sliding manifold.

Lemma 1. (*Fractional-order sliding-mode* [33]): *Consider a fractional-order system expressed by*

$$D^v x + Ax = 0,\ x(0) = x_0 \tag{13}$$

where v is the fractional-order parameter, $0 < v < 2$, $x \in R_n$, $A \in R_{n\times n}$, if $|arg(eig(A)| > v\pi/2$, and the solution of the system is asymptotically stable.

To prove the finite-time convergence of the sliding manifold, Lemma 2 is given below as the theoretical basis.

Lemma 2. (*Finite-time convergence theorem* [34]): *Consider a system $\dot{x} = f(x)$, $f(0) = 0$, $x \in R_n$, if there exists a positive definite continuous function $V(x)$: $U \to R$, real numbers $c > 0$ and $0 < \alpha < 1$, and an open neighborhood $U_0 \subset U$ of the origin such that $\dot{V} + cV^{\alpha}(x) \leq 0$, $x \in U_0\{0\}$, and then $V(x)$ can approach zero in a finite-time, $t_r \leq V^{1-\alpha}(x(0))/(c(1-\alpha))$.*

3. The Estimation Method for SoC

The SoC of the lithium battery is generally defined as the ratio of the remaining capacity to the rated capacity [35]. The SoC is related to the nature of the battery itself, but also affected by the rate of discharge, environment temperature, and ambient noise [36]. The SoC of the lithium battery is mainly defined in two ways:

(1) The electric quantity perspective-based definition is given as [35]:

$$SoC = 1 - \frac{C_s}{C_N} = 1 - \frac{\eta_s \int i_s(t)dt}{C_N} \tag{14}$$

where C_s and C_N are the discharge quantity and rated capacity of the lithium battery, $i_s(t)$ is the discharge current, and η_s is the discharge efficiency factor.

(2) The energy perspective-based definition is shown by [37]:

$$SoC = 1 - \frac{W_s}{W_N} = 1 - \frac{\eta_s \int V(t) i_s(t)dt}{W_N} \tag{15}$$

where W_s and W_N are the released energy and total energy of the lithium battery, and $V(t)$ is the terminal voltage.

In the paper, the SoC definition based on the electric quantity perspective is selected. To estimate SoC, three observers estimating the terminal voltage V_t, the open-circuit voltage V_{oc}, and the polarization voltage V_p are designed, respectively.

3.1. Terminal Voltage Observer

According to (4), an observer for V_t is proposed as follows:

$$\dot{\hat{V}}_t = -a_1 \hat{V}_t + a_1 \hat{V}_{oc}(Z) + R_t \dot{I} + b_1 I + v_1 \tag{16}$$

where v_1 is the observer control signal. The estimating error of the V_t is defined as $e_1 = V_t - \hat{V}_t$, which can be obtained from (4) and (16). Then, the dynamics of the estimation error can be expressed as:

$$\dot{e}_1 = -a_1 e_1 + a_1 \left(V_{oc} - \hat{V}_{oc}\right) - v_1 \tag{17}$$

A fractional-order sliding manifold is selected as:

$$s_1 = D^{\alpha+1} e_1 + \beta_1 e_1 \tag{18}$$

where $\beta_1 > 0$ is a constant, and α satisfies $0 < \alpha < 1$.

Theorem 1. *The finite-time convergence of the error dynamics (17) is guaranteed if the fractional-order sliding manifold (18) is utilized, and the following observer control law is designed as:*

$$v_1 = v_{1eq} + v_{1n} \tag{19}$$

$$v_{1eq} = -a_1 e_1 + D^{-\alpha}(\beta_1 e_1) \tag{20}$$

$$v_{1n} = D^{-\alpha-1}(k_1 sgn(s_1)) \tag{21}$$

where $k_1 = a_1 F_{oc} + \eta_1$, F_{oc} *is defined in (8), and* η_1 *is a positive constant. On the fractional-order sliding manifold, the estimation error of the open-circuit voltage* $e_2 = V_{oc} - \hat{V}_{oc}$ *satisfies:*

$$e_2 = D^{-\alpha-1}((k_1/a_1)sgn(s_1)) \tag{22}$$

The proof is set out in Appendix A. In conclusion, the terminal voltage V_t can be estimated directly, and the open circuit voltage V_{oc} is unknown from (4). The observer control law (19) is applied to guarantee the convergence of e_1. Although the V_{oc} is unknown, the error $e_2 = V_{oc} - \hat{V}_{oc}$ can be obtained by (22), which is further adopted for the observer of V_{oc}.

3.2. Open-Circuit Voltage Observer

According to (5), an observer for the open-circuit voltage is designed as:

$$\dot{\hat{V}}_{oc} = \kappa a_2 \hat{V}_t - \kappa a_2 \hat{V}_{oc} - \kappa a_2 \hat{V}_p + v_2 \tag{23}$$

where $\hat{V}_p$ is the estimation of V_p, v_2 the observer control law.

Defining the voltage error between V_p and its estimation as $e_3 = V_p - \hat{V}_p$, the error dynamics of the V_{oc} can be expressed based on (5) and (23) as:

$$\dot{e}_2 = \kappa a_2 e_1 - \kappa a_2 e_2 - \kappa a_2 e_3 - v_2 \tag{24}$$

A fractional-order sliding manifold is constructed by:

$$s_2 = D^{\alpha+1} e_2 + \beta_2 e_2 \tag{25}$$

where $\beta_2 > 0$ is a constant, and α satisfies $0 < \alpha < 1$.

Theorem 2. *The error dynamics (24) can approach* $s_2 = 0$ *in finite time, then converge to zero along* $s_2 = 0$ *if the fractional-order sliding manifold* s_2 *is chosen as (25) and the observer control law is designed as:*

$$v_2 = v_{2eq} + v_{2n} \tag{26}$$

$$v_{2eq} = \kappa a_2 e_1 - \kappa a_2 e_2 + D^{-\alpha}(\beta_2 e_2) \tag{27}$$

$$v_{2n} = D^{-\alpha-1}(k_2 sgn(s_2)) \tag{28}$$

where $k_2 = -\kappa a_2 F_P + \eta_2$, F_p *is a certain constant defined in (8), and* η_2 *is a positive constant. When the sliding manifold satisfies* $s_2 = 0$, *then the voltage error* e_3 *can be obtained as:*

$$e_3 = -\frac{k_2}{\kappa a_2} D^{-\alpha-1} sgn(s_2) \tag{29}$$

After the first observer (16) tracks the variable of the system (4), e_2 is given by (22) and utilized in the observer control law (26). Then, e_3 can be observed by (29) and will be transferred to the observer for V_p after e_2 converges to zero.

3.3. Polarization Voltage Observer

An observer based on the dynamics of the polarization voltage (6) can be designed by:

$$\dot{\hat{V}}_p = -a_1\hat{V}_p + b_2 I + v_3 \tag{30}$$

where v_3 is the observer control signal. Combining (6) and (30), the polarization voltage error dynamics are governed by:

$$\dot{e}_3 = -a_1 e_3 - v_3 + \Delta f \tag{31}$$

A fractional-order sliding manifold is chosen as:

$$s_3 = D^{\alpha+1}e_3 + \beta_3 e_3 \tag{32}$$

where $\beta_3 > 0$ is a constant, and α satisfies $0 < \alpha < 1$.

Theorem 3. *When the error dynamics (24) stays on the fractional-order sliding manifold $s_2 = 0$, the error dynamics (31) can reach $s_3 = 0$ in finite time and converge to zero along $s_3 = 0$, if the fractional-order sliding-mode s_3 is selected as (32) and the observer control law is presented below:*

$$v_3 = v_{3eq} + v_{3n} \tag{33}$$

$$v_{3eq} = -a_1 e_3 + D^{-\alpha}(\beta_3 e_3) \tag{34}$$

$$v_{3n} = D^{-\alpha-1}(k_3 sgn(s_3)) \tag{35}$$

where $k_3 = F_{f2} + \eta_3$, F_{f2} is from (7), $\eta_3 > 0$. When the trajectory of the error dynamics (31) reaches the sliding manifold $s_3 = 0$, we have $D^{\alpha+1}e_3 + \beta_3 e_3 = 0$, then e_3 reaches zero from Lemma 1.

From (6), we can know that only the current can be measured. When the V_{oc} in (5) is estimated, e_3 can be obtained by (29) and used in the observer control law (33). When the polarization voltage error e_3 converges to zero, all the estimation errors, i.e., e_1, e_2 and e_3, converge to zeros.

3.4. Calculation of SoC

In Theorems 1–3, three observers based on fractional-order sliding-mode theory are designed for the terminal voltage V_t, the open circuit voltage V_{oc}, and the polarization voltage V_p in the model of lithium batteries. Then, $\hat{V}_{oc}$, the estimation of V_{oc} (Z) in the second observer, is determined and can be used to calculate the SoC as follows:

$$\hat{Z} = f_{voc}^{-1}(\hat{V}_{oc}) \tag{36}$$

where f_{voc} is the known function defined in (3).

4. The Estimation Method for SoH

The estimation of SoH needs the capacity and the resistance. During the process of estimation of SoC, C_n and R_t are assumed to be constant, while in the estimation of SoH, they should be seen as variables. The definition of the SoH can be expressed in two ways.

(1) The capacity-based definition is shown by [36]:

$$\mathrm{SoH} = \frac{C_n}{C_{nom}} \tag{37}$$

where C_n and C_{nom} are the actual capacity and nominal capacity of the lithium battery.

(2) The internal resistance-based definition is given as [38]:

$$\mathrm{SoH} = \frac{R_{EoL} - R_t}{R_{EoL} - R_{nom}} \tag{38}$$

where R_t and R_{nom} are the actual and nominal resistance, and R_{EoL} is the resistance at the end of life [39]. In the SoH estimation, the capacity and resistance are monotonically changing with aging, environmental temperature, magnitude of current, and depth of discharge. The observer control signals can be viewed as continuous. Therefore, the following assumptions can be given:

$$\left|D^{\alpha}\left(\dot{I}\left(C_n^{-1} - \hat{C}_n^{-1}\right)\right)\right| + \left|D^{\alpha}\left(I\left(-\dot{C}_n C_n^{-2} + \dot{\hat{C}}_n \hat{C}_n^{-2}\right)\right)\right| \le F_c, \ \left|\dot{C}_n\right| \le F_{cn} \tag{39}$$

$$\left|D^{\alpha}\left(\dot{I}\left(R_t - \hat{R}_t\right)/R_p C_p\right)\right| + \left|D^{\alpha}\left(I\left(\dot{R}_t - \dot{\hat{R}}_t\right)/R_p C_p\right)\right| \le F_t, \ \left|\dot{R}_t\right| \le F_{rt} \tag{40}$$

where $\hat{C}_n$ and $\hat{R}_t$ are the estimation value, and F_c, F_{cn}, F_t, and F_{rt} are all known positive constants.

4.1. Battery Capacity Observer

According to the dynamics of the SoC (1), the observer can be designed as follows:

$$\dot{\hat{Z}}_{soh} = \frac{I}{\hat{C}_n} + v_4 \tag{41}$$

where $\hat{Z}_{soh}$ is the estimated variable of Z under the time-varying C_n in the design the SoH observer, and v_4 is the observer control. When e_2 converges to zero, $\hat{Z}$ is available and satisfies $\dot{\hat{Z}} = (1/C_n)I(t)$. In order to obtain C_n, $e_4 = \hat{Z} - \hat{Z}_{soh}$ is defined, then:

$$\dot{e}_4 = I\left(\frac{1}{C_n} - \frac{1}{\hat{C}_n}\right) - v_4 \tag{42}$$

A fractional-order sliding manifold is introduced as:

$$s_4 = D^{\alpha+1}e_4 + \beta_4 e_4 \tag{43}$$

where $\beta_4 > 0$ is a constant, and α satisfies $0 < \alpha < 1$.

Theorem 4. *The sliding-mode manifold is selected as (43) and the observer control law is designed as follows, then the state trajectory of the error dynamics (42) can reach $s_4 = 0$ from any $s_4(0) \neq 0$ in a finite-time $t_{4r} \le |s_4(0)|/\eta_4$:*

$$v_4 = v_{4eq} + v_{4n} \tag{44}$$

$$v_{4eq} = D^{-\alpha}(\beta_4 e_4) \tag{45}$$

$$v_{4n} = D^{-\alpha-1}(k_4 sgn(s_4)) \tag{46}$$

where $k_4 = F_c + \eta_4$, $\eta_4 > 0$. The proof is set out in Appendix A.

4.2. Battery Inner Resistance Observer

In addition to C_n, in the SoH estimation, R_t is also seen as a time varying variable. Therefore, b_1 in (4) can be rewritten as a function of C_n and R_t:

$$b_1(C_n, R_t) = 1/C_n + 1/C_p + R_t/(R_pC_p) \tag{47}$$

Different from the observer in the SoC estimation (16), another observer can be designed in the following form:

$$\dot{\hat{V}}_{tsoh} = -a_1\hat{V}_{tsoh} + a_1\hat{V}_{oc}(\hat{Z}_{soh}) + (1/\hat{C}_n + 1/C_p + \hat{R}_t/(R_pC_p))I + v_5 \tag{48}$$

where $\hat{V}_{tsoh}$ is the estimate of the terminal voltage in SoH observer, and v_5 is the observer control law. Assuming that the current of the battery cell is constant, we have $\dot{I} = 0$. Define $e_5 = V_t - \hat{V}_{tsoh}$, then:

$$\dot{e}_5 = -a_1e_5 + a_1(V_{oc}(Z) - \hat{V}_{oc}(\hat{Z}_{soh})) + (1/C_n - 1/\hat{C}_n + (R_t - \hat{R}_t)/(R_pC_p))I - v_5 \tag{49}$$

A fractional-order sliding manifold is chosen for the error dynamics (49):

$$s_5 = D^{\alpha+1}e_5 + \beta_5e_5 \tag{50}$$

where $\beta_5 > 0$ is a constant, and α satisfies $0 < \alpha < 1$.

Theorem 5. *If s_5 is chosen as (50) and the observer control law is designed as follows, the error dynamics (49) can reach $s_5 = 0$ in finite-time after the error dynamics (42) converges to zero:*

$$v_5 = v_{5eq} + v_{5n} \tag{51}$$

$$v_{5eq} = -a_1e_5 + v_{4n} + D^{-\alpha}(\beta_5e_5) \tag{52}$$

$$v_{5n} = D^{-\alpha-1}(k_5sgn(s_5)) \tag{53}$$

where$k_5 = F_t + \eta_5$, $\eta_5 > 0$. The proof is set out in Appendix A. The block diagram of the lithium battery SoC and SoH estimation method is shown in Figure 2.

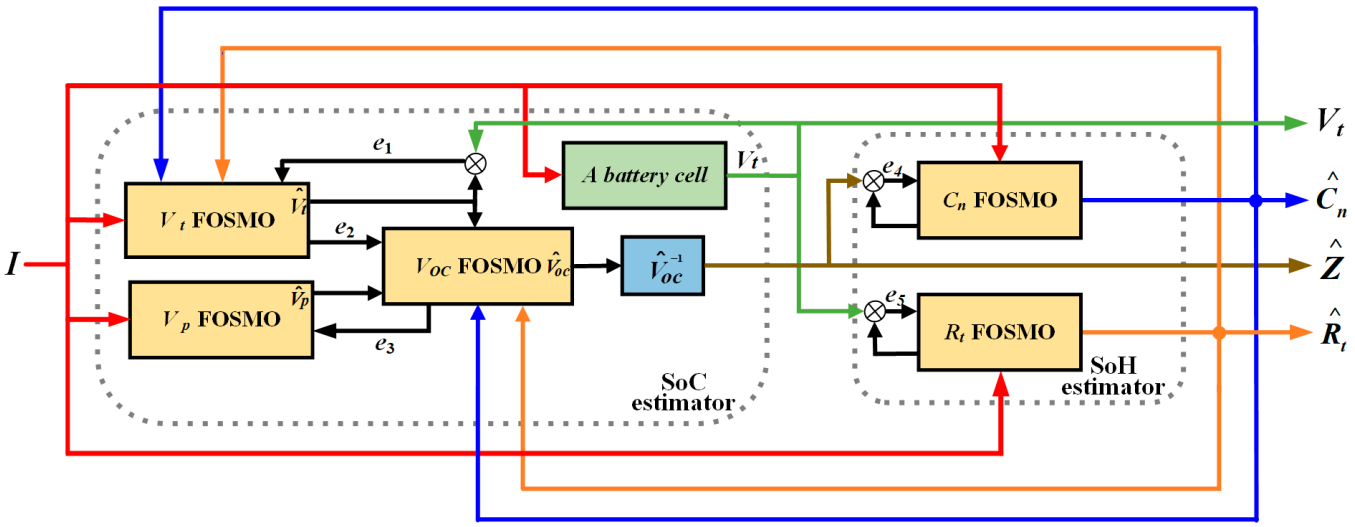

Figure 2. Block diagram of SoC and SoH algorithms.

5. Experiments

5.1. SoC-Estimation

As shown in Figure 3, the battery testing equipment consists of the Arbin BT2000 Battery Test System and the ESPEC PRA-3AP Temperature and Humidity Chamber. The Arbin BT2000 is used to record the cumulative time, voltage, current, capacity, and other data of the lithium battery. The ESPEC PRA-3AP chamber is utilized to control the temperature between −20 °C and 150 °C. The lithium battery is selected as Samsung INR 18650-20R in the paper, and the parameters are shown in the Table 1.

(**a**) (**b**)

Figure 3. The Battery testing equipment. (**a**) Arbin BT2000 battery test system. (**b**) PRA-3AP temperature and humidity chamber.

Table 1. Basic parameters of INR 18650-20R.

Symbol	Mean	Value
V_n	Nominal voltage	3.6 V
C_{nom}	Nominal capacity	2A h
V_{up}	Upper cut-off voltage	2.5 V
V_{low}	Lower cut-off voltage	4.2 V
R_p	Polarization resistance	0.0276 Ω
C_p	Polarization capacitance	1435.2 F
R_t	Ohmic resistance	0.0726 Ω

The battery tests, Dynamic Stress Test (DST) and Federal Urban Dynamic Stress Test (FUDST), are conducted to estimate the SoC of the lithium battery. The DST operating condition test is carried out according to the US Advanced Battery Consortium Battery Test Manual, which is simplified from FUDST operating conditions. It is easy to operate and effectively reflect the dynamic charging and discharging characteristics of lithium batteries. The FUDST is commonly used in industry validation tests such as to test the impact of the variable power requirements on the battery while the vehicle is in motion. The FUDST tests the car at its usual peak power condition and the high frequency of the charging and discharging process caused by acceleration and deceleration. The SoC and SoH tests of

the battery will be carried out using the above equipment under a constant temperature condition. A comparison experiment is carried out between the HOSMO and the proposed FOSMO. The sliding manifolds and the observer control laws under the HOSMO method are designed as follows:

$$\begin{cases} s_i = e_i \\ v_i = -k_{i1}|e_i|^{1/2} sgn(e_i) - k_{i2} \int sgn(e_i) dt \end{cases} \tag{54}$$

where $i = 1, 2, \cdots, 5$. When estimating the SoC, the charge and discharge current I and the terminal voltage V_t are usually estimated, which are the most basic measurement data that can be obtained. Figure 4 shows the terminal voltage V_t and the measured current I of the lithium battery from DST. In Figure 4, it can be intuitively seen that the current passing through the lithium battery basically fluctuates in the range of -4 A to 2 A, and the terminal voltage shows a trend of gradual decline. In Figure 5, the SoC state estimation of the battery was performed by DST testing. Figure 5 shows the true SoC values compared with the SoC estimation value under the FOSMO method and under the HOSMO method. Both FOSMO and HOSMO can converge to the actual values of SOC, and there is a certain drift error between the observation results and the actual value of the SOC. The FOSMO have better accuracy and faster dynamical response compared with the HOSMO method.

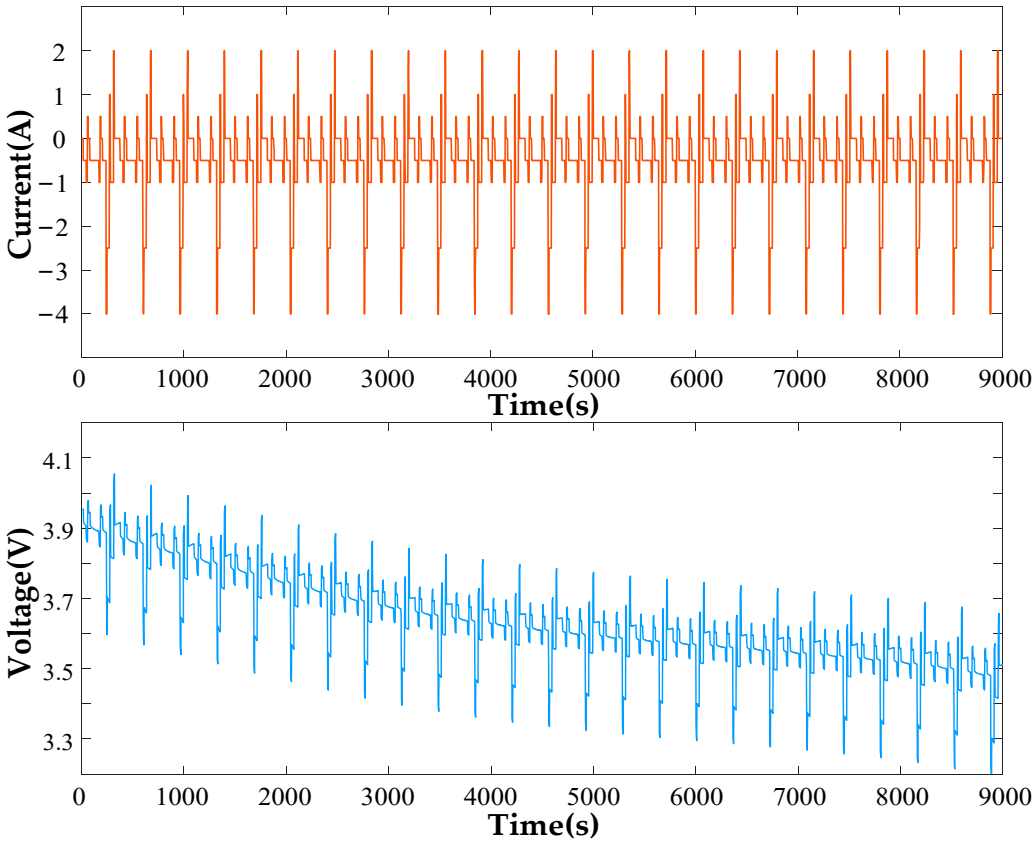

Figure 4. The current and the terminal voltage of the lithium battery from DST.

The terminal voltage V_t and the measured current I of the lithium battery under FUDST are shown in Figure 6. We can see that the rate of change of current I and terminal voltage V_t is faster under the FUDST. Figure 7 shows the actual value of the SoC compared with the estimated SoC under FOSMO and HOSMO under FUDST. In Figure 7, the estimated results under the HOSMO and FOSMO can track the actual SOC with high precision, and there is some drift error between the observed results and the actual values. The proposed method under FOSMO has a better performance in accuracy and dynamical response, and

shows much less estimation error. It is smoother than that under HOSMO, owing to the fractional-order integral observer control law.

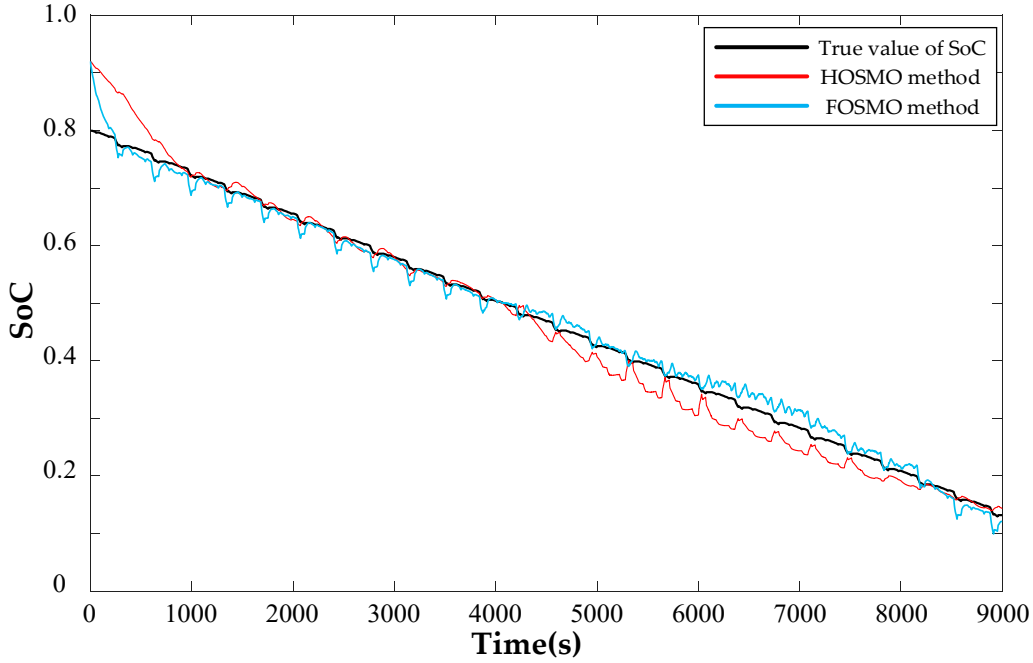

Figure 5. True value of the SoC and the estimated SoC under FOSMO and HOSMO from DST.

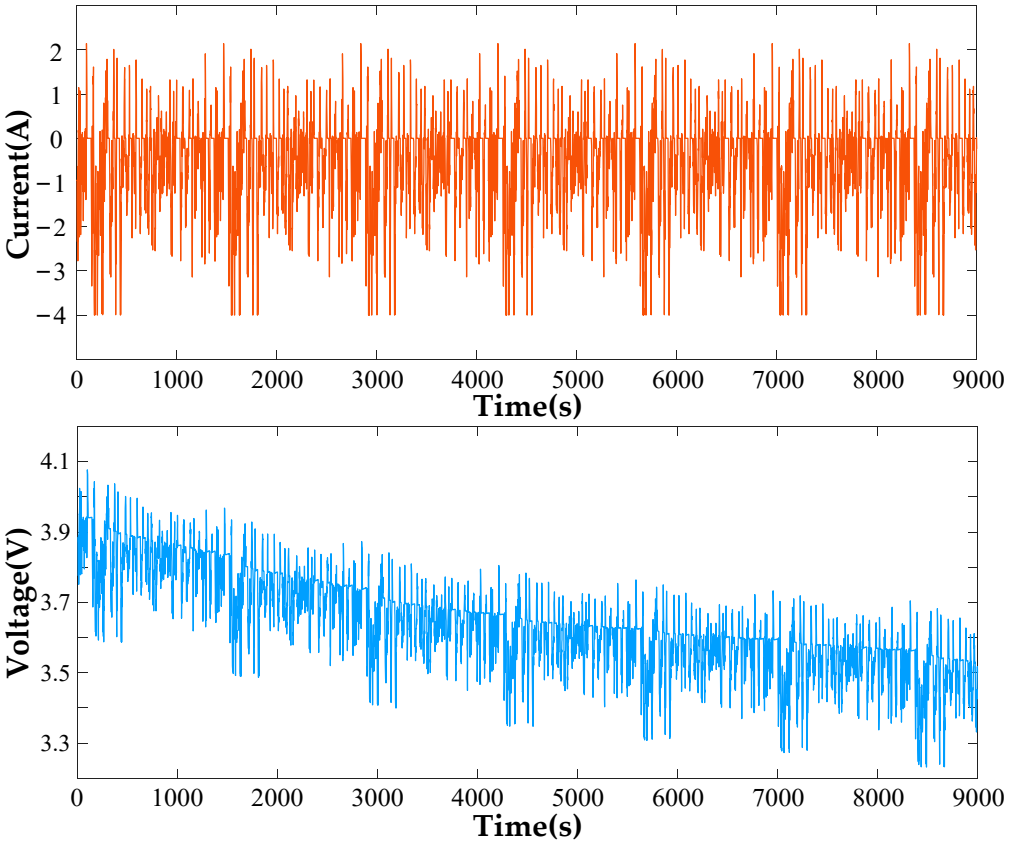

Figure 6. The current and terminal voltage of the lithium battery from FUDST.

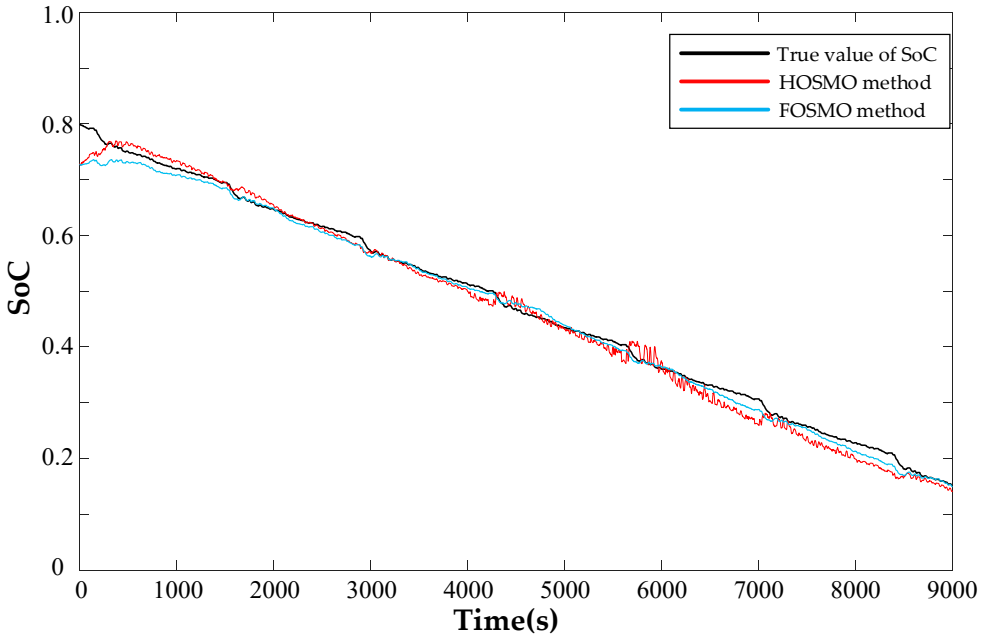

Figure 7. True value of the SoC and the estimated SoC under FOSMO and HOSMO from FUDST.

By analyzing the data in Figures 5 and 7, the estimation value of the SoC under DST and FUDST conditions are conducted with the mean absolute error (MAE), root mean squared err (RMSE), and mean relative error (MRE), as shown in Table 2. We can conclude that the real-time estimation error fluctuation in FOSMO is smaller than the HOSMO-based method, especially the RMSE and MRE, with better performance.

Table 2. The SoC estimation under the DST and FUDST testing.

Operating Condition	Method	Mean Absolute Error (MAE)	Root Mean Squared Error (RMSE)	Mean Relative Error (MRE)
DST	HOSMO	0.01536	0.02663	3.698%
	FOSMO	0.01042	0.01475	2.126%
FUDST	HOSMO	0.01436	0.01843	4.088%
	FOSMO	0.01018	0.01438	2.424%

5.2. SoH-Estimation

The SoC describes the short-term changes in current parameters. While the SoH does not need to be carried out continuously, it can be obtained by periodic measurement. The data from the INR 18650-20R cell under DST in Figure 4 is used for the SoH estimation. In this paper, the SoH algorithm is described by the battery capacity C_n and the internal resistance R_t.

In Figure 8, the real battery capacity C_n, the estimation results of capacity under FOSMO and HOSMO are depicted. It can be seen that in FUDST condition the estimates of C_n under FOSMO can converge to the real value with faster dynamical performance than that under HOSMO and fluctuate around the reference value. Furthermore, the observed results and the actual value maintain a drift error owing to the inherent error between the established mathematical model and the actual system. The estimation results of the battery's inner resistance R_t is shown in Figure 9. It shows that the estimation value of R_t under the proposed FOSMO method has better dynamic response speed and higher tracking accuracy.

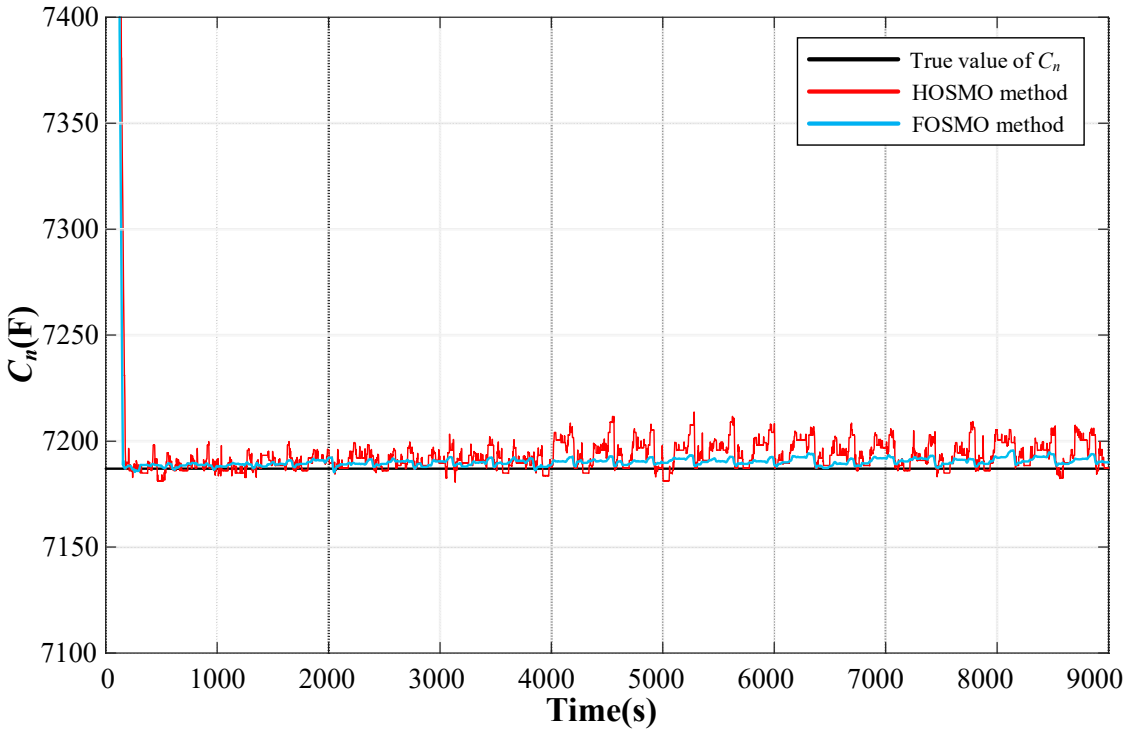

Figure 8. Comparison of C_n estimated by FOSMO and HOSMO with the true value of C_n.

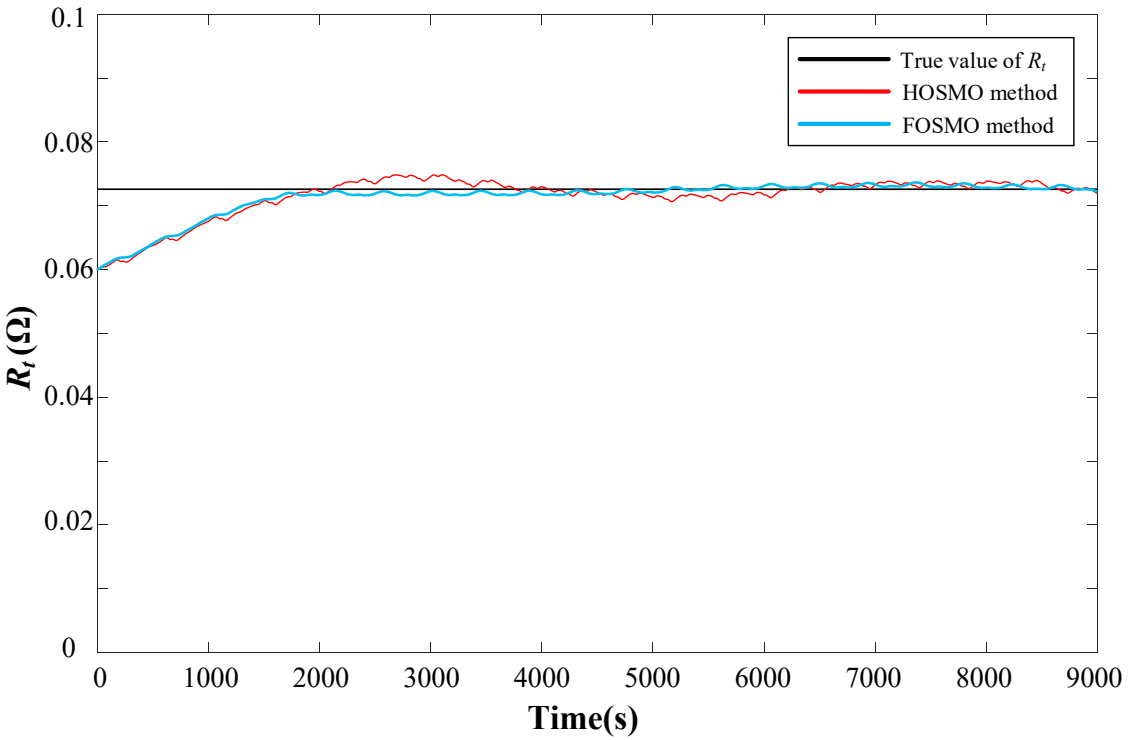

Figure 9. Comparison of R_t estimated by FOSMO and HOSMO with the true value of R_t.

According to the Figures 8 and 9, Table 3 shows the mean absolute error (MAE), root mean squared error (RMSE), and mean relative error (MRE) for the estimation value of R_t and C_n. We can conclude that, in the FOSMO method, the estimation error fluctuation is smaller than the HOSMO method. The MRE value of capacitance under FOSMO is better, which noticeably improves the performance of tracking.

Table 3. The measurement error in SoH estimation.

Test	Method	Mean Absolute Error (MAE)	Root Mean Squared Error (RMSE)	Mean Relative Error (MRE)
C_n	HOSMO	16.42 F	149.2 F	0.2582%
	FOSMO	12.49 F	109.6 F	0.1739%
R_t	HOSMO	0.001938 Ω	0.003795 Ω	2.969%
	FOSMO	0.001576 Ω	0.003108 Ω	2.073%

6. Discussion

In this paper, the fractional-order sliding-mode observers are designed for the estimation of the SoC and SoH of lithium batteries, and the corresponding experimental verifications are carried out. The SoC and SoH are the basis of the battery management system, and accurate estimation values are directly related to efficiency and safety, especially in vehicle operation. Owing to the nonlinear characteristics of battery reaction and the interference of many environmental factors, accurate estimation for the battery system is still a challenge. From the experiment result, we can see that the proposed observers have better performance in accuracy and rapidity than the HOSMO method. However, there still exist some deviations between the observed results and the actual values because of the inherent error between the established model and the actual SoC and SoH. Therefore, to design observers of higher precision, stronger robustness, and more simplification in battery management systems is our future work.

7. Conclusions

In the paper, fractional-order sliding-mode observers are proposed to estimate the SoC and SoH of the lithium cell with high accuracy and rapidity. The uncertainties, including parameter perturbations and external disturbances, are considered in the system. The main contributions of the paper can be summarized as: (1) The designed sequential connection of FOSMOs improve the global accuracy and rapidity of estimation; (2) The fractional-order sliding manifolds attenuate the chattering in the injection output signals and guarantee the smooth response of SoC; (3) The experimental tests are carried out under the DST and FUDST conditions, which verified the superiority of the proposed method compared with the existing HOSMO method.

Author Contributions: M.Z.: Conceptualization, algorithm innovation, methodology, writing and original draft; K.W.: data and formal analysis, investigation, software, simulation, writing and original draft. X.W.: conceptualization, simulation, investigation, methodology, original draft; L.W.: investigation, review, and editing; H.S.: formal analysis and editing; D.W.: project administration and writing; Y.Z. and J.L.: data and formal analysis, software, simulation. All authors have read and agreed to the published version of the manuscript.

Funding: This research was funded by the National Natural Science Foundation of China, grant number U21A20145; by the Heilongjiang Industrial Revitalization Major Project on Engineering and Science, grant number 2019ZX02A01.

Institutional Review Board Statement: Not applicable.

Informed Consent Statement: Not applicable.

Data Availability Statement: Not applicable.

Acknowledgments: This research was funded by New Energy Motor System and Key Materials Innovation Center in Harbin University of Science and Technology.

Conflicts of Interest: The authors declare no conflict of interest. The funders had no role in the design of the study; in the collection, analyses, or interpretation of data; in the writing of the manuscript; or in the decision to publish the results.

Nomenclature

V_{oc}	Open-circuit voltage
V_t	Terminal voltage
V_p	Polarization voltage
V_n	Nominal voltage
R_t	Ohmic resistance
R_p	Polarization resistance
C_p	Polarization capacitance
C_{nom}	Nominal capacity
C_n	Rated capacity if battery
Δf	Uncertainties disturbance
R_{EoL}	Resistance at the end of life
A	Fractional-order parameter
$\hat{V}_{oc}$	Estimate of open-circuit voltage
$\hat{V}_p$	Estimate of polarization voltage
$\hat{V}_t$	Estimate of terminal voltage
$\hat{R}_t$	Estimate of ohmic resistance

Appendix A

Proof of Theorem 1. Combining the dynamics of the estimation error (17) and sliding manifold (18) gives:

$$s_1 = D^{\alpha}\left(-a_1 e_1 + a_1\left(V_{oc} - \hat{V}_{oc}\right) - v_1\right) + \beta_1 e_1$$

and based on the observer control law (19) and (20), we have:

$$s_1 = D^{\alpha}\left(a_1\left(V_{oc} - \hat{V}_{oc}\right) - v_{1n}\right) \tag{A1}$$

Differentiating s_1 with respect to time t and substituting control law (21) into the above yields:

$$\begin{aligned}\dot{s}_1 &= D^{\alpha+1}\left(a_1\left(V_{oc} - \hat{V}_{oc}\right) - v_{1n}\right)\\ &= D^{\alpha+1}\left(a_1\left(V_{oc} - \hat{V}_{oc}\right)\right) - D^{\alpha+1}v_{1n}\\ &= D^{\alpha+1}\left(a_1\left(V_{oc} - \hat{V}_{oc}\right)\right) - k_1 sgn(s_1)\end{aligned}$$

Choose a Lyapunov function $V_1 = 0.5s_1^2$, then the derivative of V_1 is:

$$\begin{aligned}\dot{V}_1 = s_1\dot{s}_1 &= a_1 D^{\alpha+1}\left(V_{oc} - \hat{V}_{oc}\right)s_1 - k_1 sgn(s_1)s_1\\ &\le a_1\left|D^{\alpha+1}\left(V_{oc} - \hat{V}_{oc}\right)\right||s_1| - k_1|s_1|\\ &\le \left(a_1\left|D^{\alpha+1}\left(V_{oc} - \hat{V}_{oc}\right)\right| - k_1\right)|s_1|\end{aligned}$$

i.e., $\dot{V}_1 \le -\eta_1\sqrt{2}V_1^{1/2}$. According to Lemma 2, the error dynamics (17) can reach $s_1 = 0$ at $t_{1r} \le |s_1(0)|/\eta_1$ and maintain on it, then converge to zero based on Lemma 1. Owing to $s_1 = 0$, from (21) and (A1) we get:

$$e_2 = V_{oc} - \hat{V}_{oc} = v_{1n}/a_1 = D^{-\alpha-1}((k_1/a_1)sgn(s_1))$$

This completes the proof. □

Proof of Theorem 2. Substituting the voltage error dynamics (24) into the fractional-order sliding manifold (25) gives:

$$s_2 = D^{\alpha}(\kappa a_2 e_1 - \kappa a_2 e_2 - \kappa a_2 e_3 - v_2) + \beta_2 e_2$$

When the error dynamics (17) completes the ideal sliding motion, the observation error of V_{oc} is calculated by (22). Hence, combining (26) and (27), it can be expressed by:

$$s_2 = D^{\alpha}(-\kappa a_2 e_3 - v_{2n}) \tag{A2}$$

Differentiating s_2 and substituting the control law (28) into it gives:

$$\dot{s}_2 = D^{\alpha+1}(-\kappa a_2 e_3 - v_{2n}) = -\kappa a_2 D^{\alpha+1} e_3 - k_2 sgn(s_2)$$

Considering a Lyapunov function, $V_2 = 0.5{s_2}^2$, the derivative of V_2 is expressed as:

$$\begin{aligned} \dot{V}_2 = s_2 \dot{s}_2 &= -\kappa a_2 s_2 D^{\alpha+1} e_3 - k_2 sgn(s_2) s_2 \\ &\leq -\kappa a_2 \left| D^{\alpha+1} e_3 \right| |s_2| - k_2 |s_2| \end{aligned}$$

Based on (28), it can be obtained that $\dot{V}_2 \leq -\eta_2 \sqrt{2} {V_2}^{1/2}$. The error dynamics (24) can arrive at $s_2 = 0$ based on Lemma 2, and then converge to zero from Lemma 1. Then we have the following from (A2):

$$e_3 = V_p - \hat{V}_p = -\frac{v_{2n}}{\kappa a_2} = -\frac{k_2}{\kappa a_2} D^{-\alpha-1} sgn(s_2)$$

This completes the proof. □

Proof of Theorem 3. Based on (31) and (32):

$$s_3 = D^{\alpha}(-a_1 e_3 - v_3 + \Delta f) + \beta_3 e_3$$

When the error dynamics (24) take place $s_3 = 0$, the error voltage e_3 can be obtained as (29). Accordingly, combining (33) and (34), the above equation can be rewritten as:

$$s_3 = D^{\alpha}(-v_{3n} + \Delta f)$$

Differentiating s_3 and substituting the control law (35) into the above yields:

$$\dot{s}_3 = -D^{\alpha+1} v_{3n} + D^{\alpha+1} \Delta f = -k_3 sgn(s_3) + D^{\alpha+1} \Delta f$$

A Lyapunov function $V_3 = 0.5{s_3}^2$ is considered. From (35), the derivative of V_3 is expressed as:

$$\begin{aligned} \dot{V}_3 = s_3 \dot{s}_3 &= -s_3 D^{\alpha+1} v_{3n} + s_3 D^{\alpha+1} \Delta f \\ &= -k_3 s_3 sgn(s_3) + s_3 D^{\alpha+1} \Delta f \\ &\leq -k_3 |s_3| + |s_3| \left| D^{\alpha+1} \Delta f \right| \end{aligned}$$

i.e., $\dot{V}_3 \leq -\eta_3 \sqrt{2} V_3^{1/2}$, which means that the error dynamics (31) reaches $s_3 = 0$ in a finite-time $t_{3r} \leq |s_3(0)| / \eta_3$, and maintains $s_3 = 0$ all the time according to Lemma 2.

This completes the proof. □

Proof of Theorem 4. Based on (42) and (43):

$$s_4 = D^{\alpha}\left(I\left(C_n^{-1} - \hat{C}_n^{-1} \right) - v_4 \right) + \beta_4 e_4 \tag{A3}$$

from (44) and (45), the above becomes:

$$s_4 = D^{\alpha}\left(I\left(C_n^{-1} - \hat{C}_n^{-1} \right) - v_{4n} \right) \tag{A4}$$

differentiating s_4 above with respect to time t and substituting the control law (46) into the above yields:

$$\begin{aligned}\dot{s}_4 &= D^{\alpha}\left(\dot{I}\left(C_n^{-1}-\hat{C}_n^{-1}\right)+I\left(-\dot{C}_nC_n^{-2}+\dot{\hat{C}}_n\hat{C}_n^{-2}\right)-\dot{v}_{4n}\right)\\ &= D^{\alpha}\left(\dot{I}\left(C_n^{-1}-\hat{C}_n^{-1}\right)+I\left(-\dot{C}_nC_n^{-2}+\dot{\hat{C}}_n\hat{C}_n^{-2}\right)\right)-k_4sgn(s_4)\end{aligned} \tag{A5}$$

A Lyapunov function for the error dynamics $V_4 = 0.5{s_4}^2$ is considered, then the derivative of V_4 can be obtained as:

$$\begin{aligned}\dot{V}_4 &= s_4\dot{s}_4 = s_4D^{\alpha}\left(\dot{I}\left(C_n^{-1}-\hat{C}_n^{-1}\right)+I\left(-\dot{C}_nC_n^{-2}+\dot{\hat{C}}_n\hat{C}_n^{-2}\right)\right)-s_4k_4sgn(s_4)\\ &\le |s_4|\left|D^{\alpha}\left(\dot{I}\left(C_n^{-1}-\hat{C}_n^{-1}\right)\right)\right|+|s_4|\left|D^{\alpha}\left(I\left(-\dot{C}_nC_n^{-2}+\dot{\hat{C}}_n\hat{C}_n^{-2}\right)\right)\right|-k_4|s_4|\end{aligned}$$

i.e., $\dot{V}_4 \le -\eta_4\sqrt{2}V_4^{1/2}$, which means that the error dynamics (42) can approach $s_4 = 0$ in a finite time $t_{4r} \le |s_4(0)|/\eta_4$ according to Lemma 2. When $s_4 = 0$, from (A4) we have:

$$\frac{1}{C_n}-\frac{1}{\hat{C}_n}=\frac{v_{4n}}{I}$$

Define the error of the capacity $e_{cn} = C_n - \hat{C}_n$, then the signum function of the e_{cn} is:

$$\begin{aligned}sgn(e_{cn}) = sgn(C_n-\hat{C}_n) &= -sgn(\tfrac{1}{C_n}-\tfrac{1}{\hat{C}_n}) = -sgn(\tfrac{v_{4n}}{I})\\ &= -sgn(\tfrac{k_4}{I}D^{-\alpha-1}sgns_4)\end{aligned}$$

The estimation of C_n is designed by:

$$\dot{\hat{C}}_n = -(F_{cn}+k_{cn})sgn(\frac{k_4}{I}D^{-\alpha-1}sgns_4) = (F_{cn}+k_{cn})sgn(e_{cn}) \tag{A6}$$

where k_{cn} is a positive constant, F_{cn} is defined in (39), and the derivative of e_{cn} is expressed as:

$$\dot{e}_{cn} = \dot{C}_n - \dot{\hat{C}}_n = \dot{C}_n - (F_{cn}+k_{cn})sgn(e_{cn})$$

A Lyapunov function $V_{cn} = 0.5e_{cn}^2$ is considered, and its derivative is shown below:

$$\begin{aligned}\dot{V}_{cn} &= e_{cn}\dot{e}_{cn} = e_{cn}\dot{C}_n - e_{cn}(F_{cn}+k_{cn})sgn(e_{cn})\\ &\le |e_{cn}|\left|\dot{C}_n\right| - |e_{cn}|(F_{cn}+k_{cn}) \le -k_{cn}|e_{cn}| < 0\end{aligned}$$

which means that e_{cn} can converge to zero from $e_{cn}(0) \neq 0$ in finite time based on the Lemma 2, and $\hat{C}_n$ in (A6) can track C_n in finite time, i.e., $\hat{C}_n = C_n$.
This completes the proof. □

Proof of Theorem 5. When e_4 converges to zero, $\hat{Z}_{soh} = \hat{Z}$ can be obtained and notice that $\hat{Z} = Z$. Hence, we have $\hat{V}_{oc}(\hat{Z}_{soh}) = V_{oc}(Z)$, and the error dynamics (49) becomes:

$$\dot{e}_5 = -a_1e_5 + \left(1/C_n - 1/\hat{C}_n + \left(R_t-\hat{R}_t\right)/\left(R_pC_p\right)\right)I - v_5 \tag{A7}$$

substituting (51), (52), and (A7) into (50) gives:

$$\begin{aligned}s_5 &= D^{\alpha}\left(-a_1e_5+\left(\tfrac{1}{C_n}-\tfrac{1}{\hat{C}_n}+\tfrac{R_t-\hat{R}_t}{R_pC_p}\right)I-v_5\right)+\beta_5e_5\\ &= D^{\alpha}\left(\left(1/C_n-1/\hat{C}_n+\left(R_t-\hat{R}_t\right)/\left(R_pC_p\right)\right)I-v_{4n}-v_{5n}\right)\end{aligned}$$

After (42) reaches the sliding motion $s_4 = 0$, we have $1/C_n - 1/\hat{C}_n = u_{4n}/I$ and yield:

$$s_5 = D^{\alpha}\left(I\left(R_t - \hat{R}_t\right)/\left(R_pC_p\right) - v_{5n}\right) \tag{A8}$$

Differentiating s_5 with respect to time t gives:

$$\begin{aligned}\dot{s}_5 &= D^{\alpha+1}\left(I\left(R_t - \hat{R}_t\right)/\left(R_pC_p\right) - v_{5n}\right)\\ &= D^{\alpha}\left(\dot{I}\left(R_t - \hat{R}_t\right)/R_pC_p\right) + D^{\alpha}\left(I\left(\dot{R}_t - \dot{\hat{R}}_t\right)/R_pC_p\right) - k_5 sgn(s_5)\end{aligned}$$

Considering a Lyapunov function $V_5 = 0.5{s_5}^2$ and taking the derivative of V_5, we get

$$\begin{aligned}\dot{V}_5 &= s_5\dot{s}_5\\ &= s_5D^{\alpha}\left(\dot{I}\left(R_t - \hat{R}_t\right)/R_pC_p\right) + s_5D^{\alpha}\left(I\left(\dot{R}_t - \dot{\hat{R}}_t\right)/R_pC_p\right) - s_5k_5sgn(s_5)\\ &\le |s_5|\left|D^{\alpha}\left(\dot{I}\left(R_t - \hat{R}_t\right)/R_pC_p\right)\right| + |s_5|\left|D^{\alpha}\left(I\left(\dot{R}_t - \dot{\hat{R}}_t\right)/R_pC_p\right)\right| - k_5|s_5|\end{aligned}$$

which proves that the error dynamics (49) can hit $s_5 = 0$ in a finite time $t_{5r} \le |s_5(0)|/\eta_5$ based on Lemma 2. On the ideal fractional-order sliding-mode manifold $s_5 = 0$, from (a-8) we can define the battery inner resistance error as:

$$e_{rt} = R_t - \hat{R}_t = \frac{R_pC_p}{I}v_{5n}$$

Considering observer control law (53), we have:

$$e_{rt} = \frac{R_pC_p}{I}D^{-\alpha-1}(k_5sgn(s_5))$$

The estimation of R_t can be obtained by:

$$\dot{\hat{R}}_t = (F_{rt} + k_r)sgn\left(\frac{R_pC_p}{I}D^{-\alpha-1}(k_5sgn(s_5))\right) = (F_{rt} + k_r)sgn(e_{rt}) \tag{A9}$$

where k_r is a positive constant, and F_{rt} is defined in (40). If a Lyapunov function is chosen as $V_{tr} = 0.5e_{rt}^2$, then it can be deduced as:

$$\begin{aligned}\dot{V}_{rt} &= e_{rt}\dot{e}_{rt}\\ &= e_{rt}\left(\dot{R}_t - (F_{rt} + k_r)sgn(e_{rt})\right) \le -k_r|e_{rt}| < 0\end{aligned}$$

which can be concluded that e_{rt} can converge to zero from $e_{rt}(0) \neq 0$ and $\hat{R}_t$ in (A9) can track R_t in finite time, i.e., $\hat{R}_t = R_t$.
This completes the proof. □

References

1. Yang, H.; Wang, P.L.; An, Y.B.; Shi, C.L.; Sun, X.Z.; Wang, K.; Zhang, X. Remaining useful life prediction based on denoising technique and deep neural network for lithium-ion capacitors. *eTransportation* **2020**, *5*, 1168–2590. [CrossRef]
2. Jamal, H.; Khan, F.; Si, H.R.; Kim, J.H. Enhanced compatibility of a polymer-based electrolyte with Li-metal for stable and dendrite-free all-solid-state Li-metal batteries. *J. Mater. Chem. A* **2021**, *9*, 27304–27319. [CrossRef]
3. Zhang, W.; Wang, L.; Wang, L.; Liao, C.; Zhang, Y. Joint state-of-charge and state-of-available-power estimation based on the online parameter identification of lithium-ion battery model. *IEEE Trans. Ind. Electron.* **2022**, *69*, 3677–3688. [CrossRef]
4. Bhat, C.; Channegowda, J.; Chaudhari, S.; Naraharisetti, K. Accurate equivalent circuit parameter estimation using electrochemical battery modelling for pulsed load applications. In Proceedings of the 2021 IEEE Mysore Sub Section International Conference (MysuruCon), Hassan, India, 24–25 October 2021.

5. Feng, W.; Joseph, Y.; Kaushini, S.W.; William, M.; Javad, S.; Emanuel, T. Epitaxial Al-InAs heterostructures as platform for Josephson junction field-effect transistor logic devices. *IEEE Trans. Electron Devices* **2021**, *68*, 1524–1529.
6. Wang, Y.J.; Wang, L.; Li, M.; Chen, Z.H. A review of key issues for control and management in battery and ultra-capacitor hybrid energy storage systems. *eTransportation* **2020**, *4*, 1168–2590. [CrossRef]
7. Khan, F.; Oh, M.; Kim, J.H. N-functionalized graphene quantum dots: Charge transporting layer for high-rate and durable Li4Ti5O12-based Li-ion battery. *Chem. Eng. J.* **2019**, *369*, 1024–1033. [CrossRef]
8. Siddhartha, R.S.R.; Feng, W.; Ravi, P.; Vivek, D.; Jaydeep, P.K. High noise margin, digital logic design using josephson junction field-effect transistors for cryogenic computing. *IEEE Trans. Appl. Superconduct.* **2021**, *31*, 1–5.
9. Shrivastava, P.; Soon, T.K.; Idris, M.Y.I.B.; Mekhilef, S.; Adnan, S.B.R.S. Combined state of charge and state of energy estimation of lithium-ion battery using dual forgetting factor-based adaptive extended lalman filter for electric vehicle applications. *IEEE Trans. Veh. Technol.* **2021**, *70*, 1200–1215. [CrossRef]
10. Feng, Y.; Xue, C.; Han, Q.; Han, F.; Du, J. Robust estimation for state-of-charge and state-of-health of lithium-ion batteries using integral-type terminal sliding-mode observers. *IEEE Trans. Ind. Electron.* **2020**, *67*, 4013–4023. [CrossRef]
11. Wei, Z.; Dong, G.; Zhang, X.; Pou, J.; Quan, Z.; He, H. Model identification and state-of-charge estimation for lithium-ion battery using bilinear parameterization. *IEEE Trans. Ind. Electron.* **2021**, *68*, 312–323. [CrossRef]
12. Tanvir, R.T.; Eric, J.D.; Lee, K.W.; Chinh, D.H. Advanced diagnostics to evaluate heterogeneity in lithium-ion battery modules. *eTransportation* **2020**, *3*, 1168–2590.
13. Lorenzo, M.F.; Bhonsle, S.P.; Arena, C.B.; Davalos, R.V. Rapid impedance spectroscopy for monitoring tissue impedance, temperature, and treatment outcome during electroporation-based therapies. *IEEE Trans. Biomed. Eng.* **2021**, *68*, 1536–1546. [CrossRef]
14. Madani, S.S.; Soghrati, R.; Ziebert, C. A regression-based technique for capacity estimation of lithium-ion batteries. *Batteries* **2022**, *8*, 31. [CrossRef]
15. Yang, G.; Song, K.; Huang, X.; Wang, C.; Huang, X.; Li, J.; Zhu, C. Improved interoperability evaluation method for wireless charging systems based on interface impedance. *IEEE Trans. Power Electron.* **2021**, *36*, 8588–8592. [CrossRef]
16. Haus, B.; Mercorelli, P. Polynomial augmented extended Kalman filter to estimate the state of charge of lithium-ion batteries. *IEEE Trans. Veh. Technol.* **2020**, *69*, 1452–1463. [CrossRef]
17. He, L.; Guo, D.; Zhang, J.; Li, W.; Zheng, Y. A threshold extend Kalman filter algorithm for state of charge estimation of lithium-ion batteries in electric vehicles. *IEEE J. Emerg. Select. Top. Ind. Electron.* **2020**, *3*, 190–198. [CrossRef]
18. Galushkin, N.E.; Yazvinskaya, N.N.; Galushkin, D.N. Investigation of the temperature dependence of parameters in the generalized peukert equation used to estimate the residual capacity of traction lithium-ion batteries. *Batteries* **2022**, *8*, 280. [CrossRef]
19. Kopp, M.; Ströbel, M.; Fill, A.; Pross-Brakhage, J.; Birke, K.P. Artificial feature extraction for estimating state-of-temperature in lithium-ion-cells using various long short-term memory architectures. *Batteries* **2022**, *8*, 36. [CrossRef]
20. Doostmohammadian, M. Single-bit consensus with finite-time convergence: Theory and applications. *IEEE Trans. Aerosp. Electron. Syst.* **2020**, *56*, 3332–3338. [CrossRef]
21. Kim, I.S. A Technique for Estimating the State of Health of Lithium Batteries through a Dual-Sliding-Mode Observer. *IEEE Trans. Power Electron.* **2010**, *25*, 1013–1022.
22. Alexander, B.; Anderson, H.; Joshua, T. Study on the effect of solar irradiance intermittency mitigation on electric vehicle battery lifetime. In Proceedings of the IEEE Conference on Technologies for Sustainability, Portland, OR, USA, 1–2 August 2013; pp. 262–267.
23. Mukhopadhyay, S.; Usman, H.M.; Rehman, H. Real time li-ion battery bank parameters estimation via universal adaptive stabilization. *IEEE Open J. Control Syst.* **2022**, *1*, 268–293. [CrossRef]
24. Alexander, P.S.; Matthias, B.; Árpád, W.I. Model-based distinction and quantification of capacity loss and rate capability fade in Li-ion batteries. *J. Power Sources* **2020**, *195*, 7634–7638.
25. Domenico, D.; Stefanopoulou, A.; Fiengo, G. Lithium-ion battery state of charge and critical surface charge estimation using an electrochemical model-based extended Kalman filter. *J. Dyn. Syst. Meas. Control* **2020**, *132*, 061302. [CrossRef]
26. Anudeep, M.; Kim, J.Y.; Carney, K.; DuBois, P. Modeling extreme deformations in lithium batteries. *eTransportation* **2020**, *4*, 1168–2590.
27. Feng, X.N.; Merla, Y.; Weng, C.H.; Ouyang, M.G.; He, X.M.; Liaw, B.Y.; Santhanagopalan, S.; Li, X.M. A reliable approach of differentiating discrete sampled data for battery diagnosis. *eTransportation* **2020**, *3*, 1168–2590. [CrossRef]
28. Morstyn, T.; Savkin, A.V.; Hredzak, B.; Agelidis, V.G. Multi-agent sliding mode control for state of charge balancing between battery energy storage systems distributed in a dc microgrid. *IEEE Trans. Smart Grid.* **2018**, *9*, 4735–4743. [CrossRef]
29. Gao, Y.; Liu, K.; Zhu, C.; Zhang, X.; Zhang, D. Co-estimation of state-of-charge and state-of-health for lithium-ion batteries using an enhanced electrochemical model. *IEEE Trans. Ind. Electron.* **2022**, *69*, 2684–2696. [CrossRef]
30. Levant, A.; Alelishvili, L. Integral High-Order Sliding Modes. *IEEE Trans. Autom. Control* **2007**, *52*, 1278–1282. [CrossRef]
31. Obeid, H.; Laghrouche, S.; Fridman, L.; Chitour, Y.; Harmouche, M. Barrier function-based adaptive super-twisting controller. *IEEE Trans. Autom. Control* **2020**, *65*, 4928–4933. [CrossRef]
32. Obeid, H.; Petrone, R.; Chaoui, H.; Gualous, H. Higher order sliding-mode observers for state-of-charge and state-of-health estimation of lithium-ion batteries. *IEEE Trans. Veh. Technol.* **2022**. [CrossRef]

33. Tang, Y.G.; Zhang, X.Y.; Zhang, D.L.; Zhao, G.; Guan, X.P. Fractional order sliding mode controller design for antilock braking systems. *Neurocomputing* **2013**, *111*, 122–130. [CrossRef]
34. Feng, Y.; Han, F.L.; Yu, X.H. Chattering free full-order sliding-mode control. *Automatica* **2014**, *50*, 1310–1314. [CrossRef]
35. Zhao, X.B. *Research on On-Line State-of-Charge Estimation Technology of Lithium-Ion Battery*; Nanjing University of Aeronautics and Astronaut: Nanjing, China, 2016; pp. 45–48.
36. He, Z.; Yang, Z.; Cui, X.; Li, E. A method of state-of-charge estimation for EV power lithium-ion battery using a novel adaptive extended Kalman filter. *IEEE Trans. Veh. Technol.* **2020**, *69*, 14618–14630. [CrossRef]
37. Lin, C.; Tang, A.H.; Xing, J. Evaluation of electrochemical models-based battery state-of-charge estimation approaches for electric vehicles. *Appl. Energy* **2017**, *207*, 394–404. [CrossRef]
38. Zou, Y.; Hu, X.; Ma, H.; Li, S.E. Combined state of charge and state of health estimation over lithium-ion battery cell cycle lifespan for electric vehicles. *J. Power Sources* **2015**, *273*, 793–803. [CrossRef]
39. Goh, T.; Park, M.; Koo, G.; Seo, M.; Kim, S.W. State-of-health estimation algorithm of Li-ion battery using impedance at low sampling rate. In Proceedings of the IEEE PES Asia-Pacifific Power and Energy Engineering Conference, Xi'an, China, 25–28 October 2016.